

Glucose-Responsive Sequential Generation of Hydrogen Peroxide and Nitric Oxide for Synergistic Cancer Starving-Like/Gas Therapy

Wenpei Fan, Nan Lu, Peng Huang,* Yi Liu, Zhen Yang, Sheng Wang, Guocan Yu, Yijing Liu, Junkai Hu, Qianjun He, Junle Qu, Tianfu Wang,* and Xiaoyuan Chen*

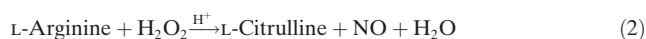
Abstract: Glucose is a key energy supplier and nutrient for tumor growth. Herein, inspired by the glucose oxidase (GOx)-assisted conversion of glucose into gluconic acid and toxic H₂O₂, a novel treatment paradigm of starving-like therapy is developed for significant tumor-killing effects, more effective than conventional starving therapy by only cutting off the energy supply. Furthermore, the generated acidic H₂O₂ can oxidize L-Arginine (L-Arg) into NO for enhanced gas therapy. By using hollow mesoporous organosilica nanoparticle (HMON) as a biocompatible/biodegradable nanocarrier for the co-delivery of GOx and L-Arg, a novel glucose-responsive nanomedicine (L-Arg-HMON-GOx) has been for the first time constructed for synergistic cancer starving-like/gas therapy without the need of external excitation, which yields a remarkable H₂O₂-NO cooperative anticancer effect with minimal adverse effect.

As an alternative to chemotherapy, the emerging gas therapy has been recognized as a “green” treatment paradigm with negligible side effects.^[1] Among the gas transmitter family, nitric oxide (NO) serves as a “star” messenger involved in a number of physiological and pathological activities.^[2] Especially in the field of cancer therapy, NO not only directly kills cancerous cells at high concentrations (> 1 μM) through the nitrosation of mitochondria and DNA,^[3] but also cooperatively enhances the efficacy of photodynamic therapy or radiotherapy.^[4] Of particular interest of NO gas therapy is to

develop biocompatible yet activatable NO donors for stimuli-responsive NO release.^[5] L-Arginine (L-Arg), a natural NO donor with excellent biocompatibility,^[6] can continuously release NO in the presence of inducible NO synthase (iNOS) enzyme.^[7] Additionally, L-Arg can also be oxidized by H₂O₂ to generate NO.^[8] It is expected that the presence of L-Arg in the H₂O₂-rich tumor microenvironment^[9] could generate a large amount of intratumoral NO for gas therapy.

Cancer starving therapy is known for blocking the nutrients supply by vascular embolization to suppress tumor growth.^[10] Alternatively, in consideration of the essential role of glucose in providing energy for tumor metabolism,^[11] we strategically starved the tumors by depleting the intratumoral glucose by a glucose-metabolic reaction, which oxidized glucose into gluconic acid and H₂O₂ using the catalysis of glucose oxidase (GOx).^[12] As we know, H₂O₂ causes malignant transformation of normal cells at endogenous concentrations,^[13] but in turn triggers cancerous cell death at high concentrations.^[14] Therefore, the consumption of intratumoral glucose by GOx is expected to increase the endogenous H₂O₂ level for cancer-killing in addition to choking off the energy supply, which contributes to the naissance of a novel paradigm of cancer starving-like therapy. Moreover, the elevated concentration of H₂O₂ is helpful to accelerate the oxidization of L-Arg into NO,^[8] and may even react with NO to produce highly biocidal peroxynitrite molecules (ONOO⁻) to further enhance the efficacy of NO gas therapy.^[15] As such, there are significant enhancement effects of starving-like therapy on gas therapy, which is expected to yield a remarkable H₂O₂-NO synergistic therapeutic effect.

In order to achieve synergistic cancer starving-like/gas therapy, hollow mesoporous organosilica nanoparticles (HMONs) are employed for the co-delivery of GOx and L-Arg (Figure 1 a) based on the following multifaceted considerations: First, compared with inorganic nanocarriers, HMON demonstrates better biocompatibility and biodegradability in the reductive microenvironment.^[15] Second, GOx and L-Arg are spatially separated on the surface and in the hollow cavity of HMON, respectively, allowing for a high co-loading efficiency. Thirdly, thanks to the internal cavity, HMON serves as an ultrasound (US) imaging contrast agent for positioning tumors.^[15a,16] Most importantly, GOx oxidizes intratumoral glucose into toxic H₂O₂ for the subsequent oxidization of L-Arg into NO by the following two-step reactions given in Equations (1) and (2):



[*] Dr. W. Fan, Prof. P. Huang, Dr. S. Wang, Dr. Q. He, Prof. T. Wang
Guangdong Key Laboratory for Biomedical Measurements and
Ultrasound Imaging, School of Biomedical Engineering
Shenzhen University, Shenzhen 518060 (China)
E-mail: peng.huang@szu.edu.cn
tfwang@szu.edu.cn

Dr. W. Fan, Prof. J. Qu
Key Laboratory of Optoelectronic Devices and
Systems of Ministry of Education and Guangdong Province
College of Optoelectronic Engineering, Shenzhen University
Shenzhen 518060 (China)

Dr. W. Fan, N. Lu, Dr. Y. Liu, Z. Yang, Dr. G. Yu, Dr. Y. Liu, Prof. X. Chen
Laboratory of Molecular Imaging and Nanomedicine
National Institute of Biomedical Imaging and
Bioengineering, National Institutes of Health
Bethesda, MD 20892 (USA)
E-mail: shawn.chen@nih.gov

Dr. J. Hu
Department of Chemistry & Biochemistry, University of Maryland
College Park, MD 20742 (USA)

Supporting information and the ORCID identification number(s) for the author(s) of this article can be found under <http://dx.doi.org/10.1002/anie.201610682>.

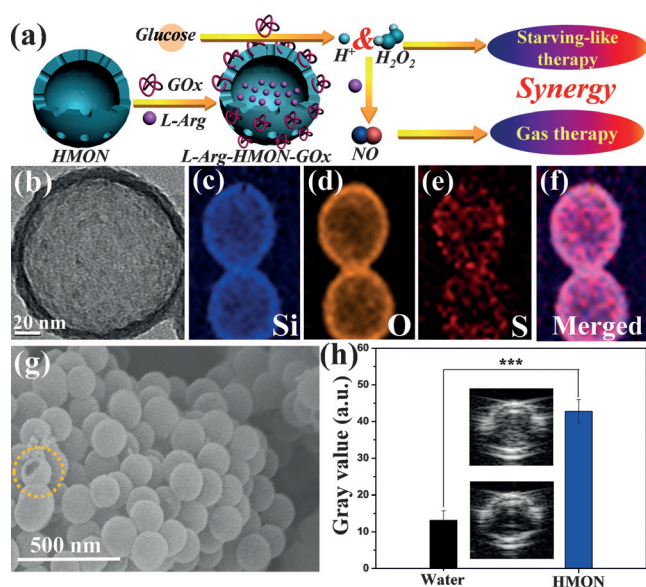


Figure 1. a) Schematic illustration of the construction of L-Arg-HMON-GOx for synergistic cancer starving-like/gas therapy. b) TEM image of a single HMON nanoparticle. c–f) Elemental mapping of HMON: c) Si, d) O, e) S, f) Mergence. g) SEM image of HMON. h) Average gray values of degassed water and HMON, and the insets are their corresponding B-mode US images of (upper) HMON and (down) water. *** $P < 0.001$.

Interestingly, the pH decrease as a result of the generated gluconic acid [Eq. (1)] also accelerates the L-Arg-H₂O₂ reaction for an increased NO yield [Eq. (2)]. Specifically, the conversion of glucose into H₂O₂ and NO for tumor growth inhibition is spontaneous without the need of external energy input. Furthermore, the developed synergistic starving-like/gas therapy may hopefully establish a novel green yet noninvasive treatment paradigm with significant clinical values, minimizing the concerns about side effects.

Herein, HMON was fabricated according to a selective etching strategy with modification (see Figure S1a in the Supporting Information). Dense SiO₂ nanoparticles (Figure S1b) were synthesized via a typical Stöber method. Due to the chemical homology between tetraethyl orthosilicate (TEOS) and bis[3-(triethoxysilyl)propyl]tetrasulfide (BTES), a disulfide-bridged mesoporous organosilica shell was coated on the surface of SiO₂ (denoted as SiO₂@MON, Figure S1c). Then HMON with a huge cavity (Figure 1b) was obtained by selectively etching away the SiO₂ core in a Na₂CO₃ solution while maintaining the outer organosilica shell intact (Figure S1d). The silica coating process took place at 80 °C using cetyltrimethylammonium chloride (CTAC) as the pore-forming agent, which saved at least 5 h in comparison to hexadecyltrimethylammonium bromide (CTAB)-assisted silica coating at room temperature in other studies.^[15a,17]

The as-synthesized HMON exhibits a spherical morphology (Figure 1g) with a narrow hydrodynamic size distribution centered at 184.3 nm (Figure S2), indicating its high dispersity without obvious aggregation. All the major elements (Si, O, S) are shown in the element mapping images (Figure 1c–f) and EDS spectrum (Figure S3). Especially, the S signal is

homogeneously distributed within the silica framework, confirming the successful disulfide hybridization (Figure S4) for HMON. After extraction of CTAC, HMON has a relatively large surface area of 293 m²g⁻¹ and pore size of 3.7 nm (Figure S5), which facilitates efficient loading of guest molecules into the hollow cavity.

The incorporation of organic thioether groups into silica frameworks may endow HMON with enhanced biological performances. As shown in Figure S6, over 95% of cells remained alive after 24 h of incubation with HMON, indicating high biocompatibility of HMON even without surface modification. By conjugation with FITC, the efficient intracellular transport of HMON via a typical endocytosis process was observed under the confocal laser scanning microscopic (Figure S7). Thanks to the huge hollow interior for scattering/reflecting US signals^[16] as well as the hybridized long-chain thioether groups for enhancing the elasticity of the silica shell to US wave,^[18] HMON could serve as a good US contrast imaging agent, which generates three-fold enhancement of B-mode US signals in comparison to water (Figure 1h). After injection into the U87MG xenograft tumor, the strong B-mode US signal (Figure S8) helps to position the tumor. Compared with other inorganic silica nanoparticles, HMON is featured with its distinct biodegradation behavior in the reductive tumor microenvironment because the disulfide bonds within the silica framework are highly sensitive to the reductive environment and easily broken down to collapse the organosilica shell. As observed in the TEM and SEM images of HMON in GSH solutions (for simulated tumor microenvironment), HMON demonstrates a time-dependent biodegradation behavior and almost all HMON particles are degraded within 30 days (Figures S9 and S10). The biodegradability of HMON is expected to enhance its biosafety, facilitate its excretion as well as accelerate the release of loaded guest molecules for better biological effects.

GOx, an enzyme with abundant carboxyl groups, was covalently conjugated onto the surface of HMON (Figure S11a) to form a “corona” without leakage (Figure S12). Meanwhile, L-Arg molecules were encapsulated into the hollow cavity of HMON through hydrogen bonding and electrostatic interactions. Therefore, GOx and L-Arg were separately conjugated onto the surface and loaded into the cavity of HMON, respectively (Figure S13), which yielded the water-dispersible L-Arg-HMON-GOx (Figure S11d). As calculated by the thermo-gravimetric analysis (TGA) of L-Arg-HMON-GOx (Figure 2a), the co-loading capacities of GOx and L-Arg are as high as 10 and 13 wt%, respectively.

Based on GOx-catalyzed decomposition reaction of glucose, we find that both the generated H₂O₂ and gluconic acid (reflected by pH) concentrations quickly reach an equilibrium within only 1 h (Figure S14a and b), which indicates the high catalytic efficiency of GOx. It is no surprise that GOx still keeps its activity after conjugation (Figure S14c and d). The generated H₂O₂ and acid concentrations are increased in response to the elevated concentrations of glucose (Figure 2b and c). To study the promoting effect of acid on the L-Arg-H₂O₂ reaction, the generated NO concentrations in neutral (pH 7.4) and acidic (pH 4.0) solutions were measured using a typical Griess assay. Although the L-Arg-

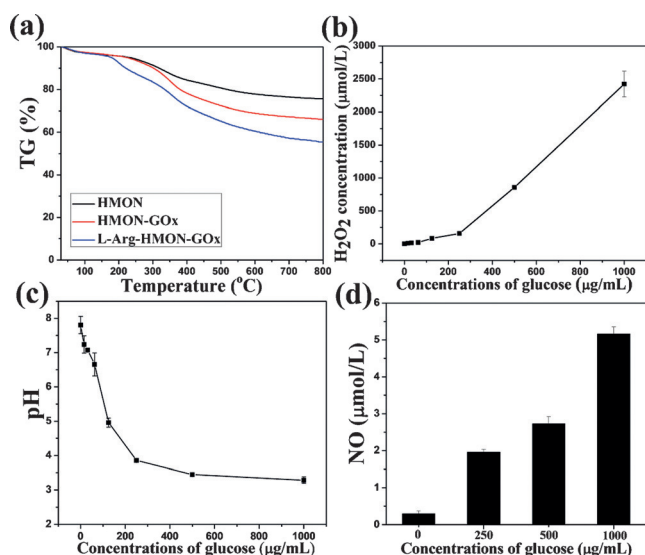


Figure 2. a) TG curves of HMON-GOx, HMON-L-Arg and L-Arg-HMON-GOx. b–c) The generated H₂O₂ concentration (b) and pH value (c) arising from the reaction between HMON-GOx and different concentrations of glucose. d) The generated NO concentrations arising from the reaction between L-Arg-HMON-GOx and different concentrations of glucose.

H₂O₂ reaction rate is very slow in neutral solutions, a burst NO release is clearly found in acidic solutions (Figure S15a), about four-fold higher than that in neutral solutions, suggesting the greatly accelerated oxidation of L-Arg by acidic H₂O₂. Meanwhile, the generated NO is also proportional to H₂O₂ concentration (Figure S15b). Taken together, via the co-loading of GOx and L-Arg into HMON, L-Arg-HMON-GOx can generate NO in glucose solutions via the oxidation of glucose into H₂O₂/H⁺ by GOx and the subsequent oxidation of L-Arg into NO by H₂O₂/H⁺. As expected, L-Arg-HMON-GOx also demonstrates glucose-dependent NO release (Figure 2d) because the generated NO amount relies on the H₂O₂/H⁺ concentration, which is related to the added glucose concentration.

To observe the intracellular NO release in vitro, a fluorogenic Rhodamine B Spirolactam-based (RhBS) NO probe (Figure S16) was used to evaluate the NO generation on U87MG cells. First, after 6 h of incubation with GOx or L-Arg loaded or GOx/L-Arg co-loaded HMON in glucose-free DMEM medium, the U87MG cells were harvested for flow cytometry analysis and fluorescence imaging. As seen in Figure 3a and b, although HMON-L-Arg can react with intracellular H₂O₂ to generate NO, a much larger amount of NO is released from L-Arg-HMON-GOx because GOx can oxidize the intracellular glucose to increase H₂O₂ concentration (Figure 3c) that accelerates the oxidation of L-Arg into NO. Meanwhile, a strong red fluorescence signal is also observed in L-Arg-HMON-GOx-treated cells (Figure S17), which further confirms the higher concentration of intracellular NO release from L-Arg-HMON-GOx than that of HMON-L-Arg. Subsequently, the intracellular NO release was measured on U87MG cells incubated with L-Arg-HMON-GOx in glucose-containing DMEM medium. As

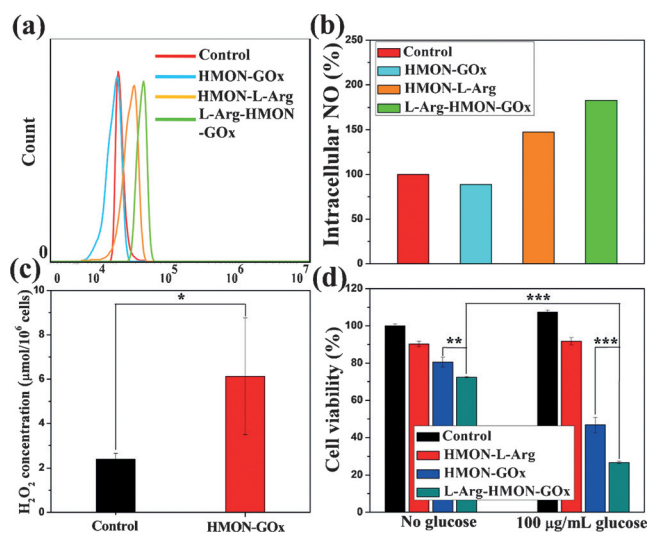


Figure 3. a) Flow cytometry analysis and b) the corresponding quantitative evaluation of intracellular NO generation (using the RhBS NO probe) in U87MG cells after being treated with HMON-GOx, HMON-L-Arg and L-Arg-HMON-GOx. The untreated cells were used as the control. c) The change of H₂O₂ level in U87MG cells after HMON-GOx treatment. d) U87MG cell viability after different treatments in the absence and presence of 100 μg mL⁻¹ glucose. **P* < 0.05, ***P* < 0.01, ****P* < 0.001.

expected, the intracellular NO level is higher with increased glucose concentrations (Figure S18 and S19), which shows the glucose-dependent NO release from L-Arg-HMON-GOx in vitro.

During the tumor growth, glucose serves as an energy supplier to promote cancerous cell proliferation (Figure S20a). As a high concentration of H₂O₂ causes significant cell death (Figure S20b), the starving-like therapy via the GOx-triggered decomposition of glucose into toxic H₂O₂ produces a much stronger anticancer effect than the conventional starving therapy which only blocks the glucose supply. Conversely and excitingly, HMON-GOx-triggered starving-like therapy results in a lower cell viability at a higher concentration of glucose (Figure S21), which should be attributed to a higher level of H₂O₂ production. Meanwhile, although HMON-L-Arg reacts with intracellular H₂O₂ to produce small amount of NO and cause marginal cell death (Figure S22), much more NO is produced at increased H₂O₂ concentrations to cause more cell death (Figure S23), thus yielding an improved gas therapeutic effect. Encouraged by the GOx-induced high H₂O₂ concentration for accelerating NO production from L-Arg, the synergistic starving-like/gas therapy can be achieved by L-Arg-HMON-GOx to cause a higher cell death rate than single starving-like therapy by HMON-GOx or gas therapy by HMON-L-Arg (Figures 3d and S24).

After validating the high biocompatibility of HMON in vivo (Figure S25), the evaluation of synergistic cancer starving-like/gas therapy was further performed on the U87MG tumor-bearing mice. By comparison with PBS group (Figure S26), the intratumoral blood oxygen saturation (sO₂) after injection of HMON-GOx quickly dropped and maintained

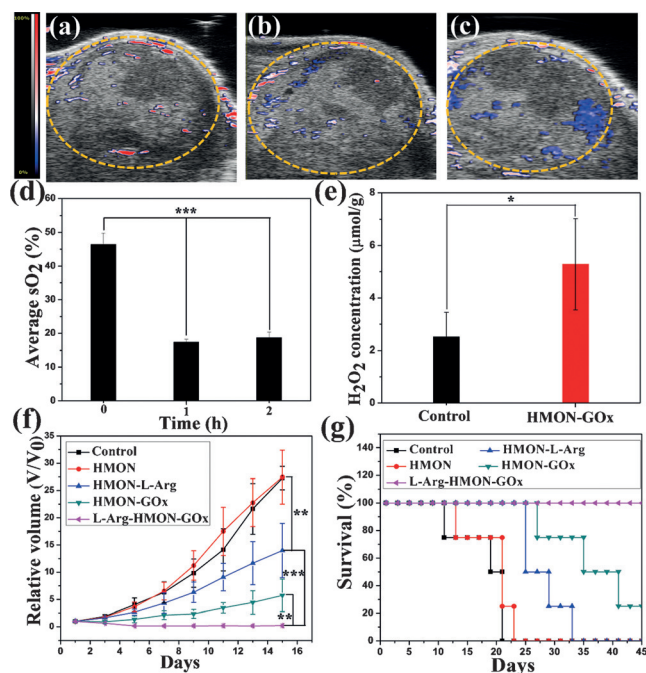


Figure 4. a–c) PA oxygen saturation mapping and US coregistered imaging of U87MG tumors a) before, b) 1 h, and c) 2 h after injection of HMON-GOx. d) Quantitative analysis of sO_2 levels in U87MG tumors before and after injection of HMON-GOx. e) The change of H_2O_2 concentrations in U87MG tumors at 4 h after injection HMON-GOx. f) Tumor growth curve and g) survival curve of U87 tumor-bearing mice after different treatments. * $P < 0.05$, ** $P < 0.01$, *** $P < 0.001$.

below 20% within 2 h (Figure 4d), as shown by the parametric “Oxyhemo” mode of PA/US coregistered imaging (Figure 4a–c). Meanwhile, HMON-GOx causes a drastic two-fold increase in intratumoral H_2O_2 concentration (Figure 4e). These findings confirm that HMON-GOx can consume the intratumoral glucose^[11] and O_2 for H_2O_2 generation, which significantly shrinks tumors and simultaneously cuts off the energy supply to starve tumors. However, HMON-L-Arg seems to be less effective in inhibiting the tumor growth (Figure S27) because of the limited intratumoral H_2O_2 concentration that oxidizes insufficient amount of L-Arg into NO for relative low gas therapy efficacy. However, after treatment with L-Arg-HMON-GOx, the tumors were remarkably eliminated (Figure 4f), presumably due to both the elevated H_2O_2 concentration arising from GOx-catalyzed decomposition of intratumoral glucose and the significantly enhanced NO gas therapy arising from H_2O_2/H^+ -triggered oxidation of L-Arg. Moreover, L-Arg-HMON-GOx results in the most significant tumor apoptosis and necrosis (Figure S28), indicating the remarkably improved synergistic starving-like/gas bimodal therapeutic effects, much better than either single treatment alone. Inspiringly, the mice after treatment with L-Arg-HMON-GOx exhibit a much longer survival life (over 45 days) than the other groups (Figure 4g), which further confirms the optimized in vivo treatment efficacy of starving-like/gas synergistic therapy. Furthermore, no significant body weight change is noticed after all the treatments (Figure S29),

which suggests L-Arg-HMON-GOx does not induce discernible toxic side effects in treated animals.

In summary, an excellent biocompatible and biodegradable HMON-based nanomedicine has been successfully constructed for the co-delivery of GOx and L-Arg. On the one hand, GOx can convert the intratumoral glucose into gluconic acid and toxic H_2O_2 for killing cancerous cells in addition to cutting off the energy supply, thus realizing the renaissance of conventional starving therapy into more effective starving-like therapy. On the other hand, the in situ generated acidic H_2O_2 can accelerate the oxidation of L-Arg for enhanced NO gas therapy. To the best of our knowledge, this is the first study to illustrate an unprecedented concept of synergistic starving-like/gas therapy, so as to yield a remarkable H_2O_2 -NO cooperative anticancer effect. Furthermore, this work may hopefully establish an endogenous, non-invasive yet green treatment paradigm based on only intratumoral glucose-responsive chemical reactions without any external intervention.

Acknowledgements

This project is financially supported by the startup fund from the Shenzhen University, the National Science Foundation of China (grant numbers 81401465, 51573096, and 51602203), the Postdoctoral Science Foundation of China (grant number 2016M590808), and the Intramural Research Program (IRP) of the NIBIB, NIH.

Conflict of interest

The authors declare no conflict of interest.

Keywords: hydrogen peroxide · mesoporous nanomaterials · nitric oxide · synergistic therapy · ultrasound imaging

How to cite: *Angew. Chem. Int. Ed.* **2017**, *56*, 1229–1233
Angew. Chem. **2017**, *129*, 1249–1253

- [1] a) J. Kang, Z. Li, C. L. Organ, C.-M. Park, C.-t. Yang, A. Pacheco, D. Wang, D. J. Lefer, M. Xian, *J. Am. Chem. Soc.* **2016**, *138*, 6336–6339; b) J. Gehring, B. Trepka, N. Klinkenberg, H. Bronner, D. Schleheck, S. Polarz, *J. Am. Chem. Soc.* **2016**, *138*, 3076–3084; c) Q. He, D. O. Kiesewetter, Y. Qu, X. Fu, J. Fan, P. Huang, Y. Liu, G. Zhu, Y. Liu, Z. Qian, X. Chen, *Adv. Mater.* **2015**, *27*, 6741–6746.
- [2] a) H. T. T. Duong, N. N. M. Adnan, N. Barraud, J. S. Basuki, S. K. Kuty, K. Jung, N. Kumar, T. P. Davis, C. Boyer, *J. Mater. Chem. B* **2014**, *2*, 5003–5011; b) M. C. Frost, M. E. Meyerhoff, *J. Am. Chem. Soc.* **2004**, *126*, 1348–1349.
- [3] a) J. Fan, N. He, Q. He, Y. Liu, Y. Ma, X. Fu, Y. Liu, P. Huang, X. Chen, *Nanoscale* **2015**, *7*, 20055–20062; b) X. Zhang, G. Tian, W. Yin, L. Wang, X. Zheng, L. Yan, J. Li, H. Su, C. Chen, Z. Gu, Y. Zhao, *Adv. Funct. Mater.* **2015**, *25*, 3049–3056; c) J. Xu, F. Zeng, H. Wu, C. Hu, C. Yu, S. Wu, *Small* **2014**, *10*, 3750–3760.
- [4] a) W. Fan, W. Bu, Z. Zhang, B. Shen, H. Zhang, Q. He, D. Ni, Z. Cui, K. Zhao, J. Bu, J. Du, J. Liu, J. Shi, *Angew. Chem. Int. Ed.* **2015**, *54*, 14026–14030; *Angew. Chem.* **2015**, *127*, 14232–14236; b) S. Ning, M. Bednarski, B. Oronsky, J. Scicinski, S. J. Knox, *Biochem. Biophys. Res. Commun.* **2014**, *447*, 537–542; c) H.-J.

- Xiang, Q. Deng, L. An, M. Guo, S.-P. Yang, J.-G. Liu, *Chem. Commun.* **2016**, 52, 148–151; d) M. De Ridder, D. Verellen, V. Verovski, G. Storme, *Nitric Oxide* **2008**, 19, 164–169.
- [5] a) H. W. Choi, J. Kim, J. Kim, Y. Kim, H. B. Song, J. H. Kim, K. Kim, W. J. Kim, *ACS Nano* **2016**, 10, 4199–4208; b) P. T. Burks, J. V. Garcia, R. Gonzalez-Irias, J. T. Tillman, M. Niu, A. A. Mikhailovsky, J. Zhang, F. Zhang, P. C. Ford, *J. Am. Chem. Soc.* **2013**, 135, 18145–18152.
- [6] R. M. J. Palmer, D. S. Ashton, S. Moncada, *Nature* **1988**, 333, 664–666.
- [7] S. Kudo, Y. Nagasaki, *J. Controlled Release* **2015**, 217, 256–262.
- [8] F. Yang, P. Chen, W. He, N. Gu, X. Zhang, K. Fang, Y. Zhang, J. Sun, J. Tong, *Small* **2010**, 6, 1300–1305.
- [9] a) W. Fan, W. Bu, B. Shen, Q. He, Z. Cui, Y. Liu, X. Zheng, K. Zhao, J. Shi, *Adv. Mater.* **2015**, 27, 4155–4161; b) Y. Kuang, K. Balakrishnan, V. Gandhi, X. Peng, *J. Am. Chem. Soc.* **2011**, 133, 19278–19281.
- [10] a) Y.-X. J. Wang, X.-M. Zhu, Q. Liang, C. H. K. Cheng, W. Wang, K. C.-F. Leung, *Angew. Chem. Int. Ed.* **2014**, 53, 4812–4815; *Angew. Chem.* **2014**, 126, 4912–4915; b) E. Jubeli, N. Yagoubi, F. Pascale, L. Bédouet, K. Slimani, D. Labarre, J. P. Saint-Maurice, A. Laurent, L. Moine, *Eur. J. Pharm. Biopharm.* **2015**, 96, 396–408; c) X. Chen, H. Lv, M. Ye, S. Wang, E. Ni, F. Zeng, C. Cao, F. Luo, J. Yan, *Int. J. Pharm.* **2012**, 426, 248–255.
- [11] O. Warburg, F. Wind, E. Negelein, *J. Gen. Physiol.* **1927**, 8, 519–530.
- [12] a) D. Liu, J. Yang, H.-F. Wang, Z. Wang, X. Huang, Z. Wang, G. Niu, A. R. Hight Walker, X. Chen, *Anal. Chem.* **2014**, 86, 5800–5806; b) C. Wang, Y. Ye, G. M. Hochu, H. Sadeghifar, Z. Gu, *Nano Lett.* **2016**, 16, 2334–2340; c) J. Yu, Y. Zhang, Y. Ye, R. DiSanto, W. Sun, D. Ranson, F. S. Ligler, J. B. Buse, Z. Gu, *Proc. Natl. Acad. Sci. USA* **2015**, 112, 8260–8265.
- [13] a) T. P. Szatrowski, C. F. Nathan, *Cancer Res.* **1991**, 51, 794–798; b) M. Lopez-Lazaro, *Faseb J.* **2006**, 20, 828–832.
- [14] a) M. López-Lázaro, *Cancer Lett.* **2007**, 252, 1–8; b) J. A. Imlay, S. M. Chin, S. Linn, *Science* **1988**, 240, 640–642.
- [15] a) Y. Chen, Q. Meng, M. Wu, S. Wang, P. Xu, H. Chen, Y. Li, L. Zhang, L. Wang, J. Shi, *J. Am. Chem. Soc.* **2014**, 136, 16326–16334; b) Y. Chen, J. Shi, *Adv. Mater.* **2016**, 28, 3235–3272.
- [16] K. Zhang, H. Chen, X. Guo, D. Zhang, Y. Zheng, H. Zheng, J. Shi, *Sci. Rep.* **2015**, 5, 8766.
- [17] Y. Chen, P. Xu, H. Chen, Y. Li, W. Bu, Z. Shu, Y. Li, J. Zhang, L. Zhang, L. Pan, X. Cui, Z. Hua, J. Wang, L. Zhang, J. Shi, *Adv. Mater.* **2013**, 25, 3100–3105.
- [18] P.-L. Lin, R. J. Eckersley, E. A. H. Hall, *Adv. Mater.* **2009**, 21, 3949–3952.

Manuscript received: November 1, 2016

Revised: November 19, 2016

Final Article published: December 9, 2016